Localization by Superposing Beats: First Laboratory Experiments and Theoretical Analyzes

Matthias Schneider
University of Rostock
18051 Rostock, Germany
matthias.schneider@ipp.mpg.de

Ralf Salomon
University of Rostock
18051 Rostock, Germany
ralf.salomon@uni-rostock.de

Abstract

Many everyday life activities require precise localization information. Navigation by means of the global positioning system (GPS) is a well-known example. Despite its broad usage, this localization method cannot be utilized in all application areas. Logistics, factory and laboratory automation, as well as warehouse management, for example, require the low-cost localization of various objects with a precision of a few centimeters, particularly in indoor environments. For this type of applications, this paper proposes a new localization procedure that is based on the superposition of particularly parameterized beats. In addition, this paper also presents a preliminary theoretical analysis as well as some laboratory experiments.

1. Introduction

During the last two decades, localization systems have been receiving increasing attention. The global positioning system (GPS) and Galileo [4] are two well-known examples. Both systems can determine the position of a receiver with a precision of about a few meters, which can be improved to a few centimeters under certain circumstances [5]. Both GPS and Galileo require a direct line-of-sight to at least four satellites in order to work properly. However, factories, laboratories, warehouses, etc. are typically *indoor* environments, which exclude GPS and Galileo to a large extent. The pertinent literature provides some variations that relieve some of the limitations mentioned above. Indoor GPS [1, 9], for example, provides a localization accuracy of about some millimeters. But due to their costs, such systems are very often not affordable in everyday life or home applications.

In general, a distance can be measured by the time-of-flight of a signal. If using electromagnetic signals, a resolution in the range of a centimeter requires a sampling rate of a little more than 3 GHz. However, with respect to low costs, this approach is currently unfeasible. Furthermore, a resolution of about a millimeter and below, will be unrealistic for low-cost devices for the near future.

Sensor networks [2] is a research area in which low-cost, high-precision localization is of particular interest [3]. A sensor network consists of a huge number of tiny sensor nodes, which are usually randomly distributed over an area of interest. All sensors [7, 6] measure pre-specified environmental conditions and propagate them by means of wireless radio capabilities to the nearest receivers, also called data sinks. Because of the required routing and the information processing done at later stages, localization plays a fundamental role, since all sensor nodes have to know their (approximate) positions. For this purpose, research on sensor networks has developed a significant number of domain-specific localization procedures [8]. However, with respect to both localization accuracy and hardware requirements, these localization procedures are not suitable for all kinds of operational areas.

For the application areas mentioned above, Section 2 proposes a new localization procedure, called localization by superposing-beats (LSB). This procedure employs at least two transmitters that emit particularly modulated beats. These modulated beats lead to envelopes of low-frequency and *location-dependent* shapes. A simple receiver can analyze these location-dependent shapes, and thus, reconstruct its own relative location Δx. Section 2 presents a detailed description of the LSB procedure as well as some of its properties.

The LSB procedure has also been investigated in some practical experiments. The results are presented in Section 3, and validate the preliminary theoretical analysis. The reconstruction of the relative position Δx requires a proper receiver, which is briefly discussed in Section 4. Essentially, such a receiver consists of a peak detector as well as a low-cost data processing module that analyzes the shape of the low-frequency envelope. Finally, Section 5 concludes with a brief discussion.

2. The Superposing-Beats Procedure

This section describes the localizatio-by-superposing-beats (LSB) procedure in detail. The presentation consists of a brief summary of some well-known preliminaries, the

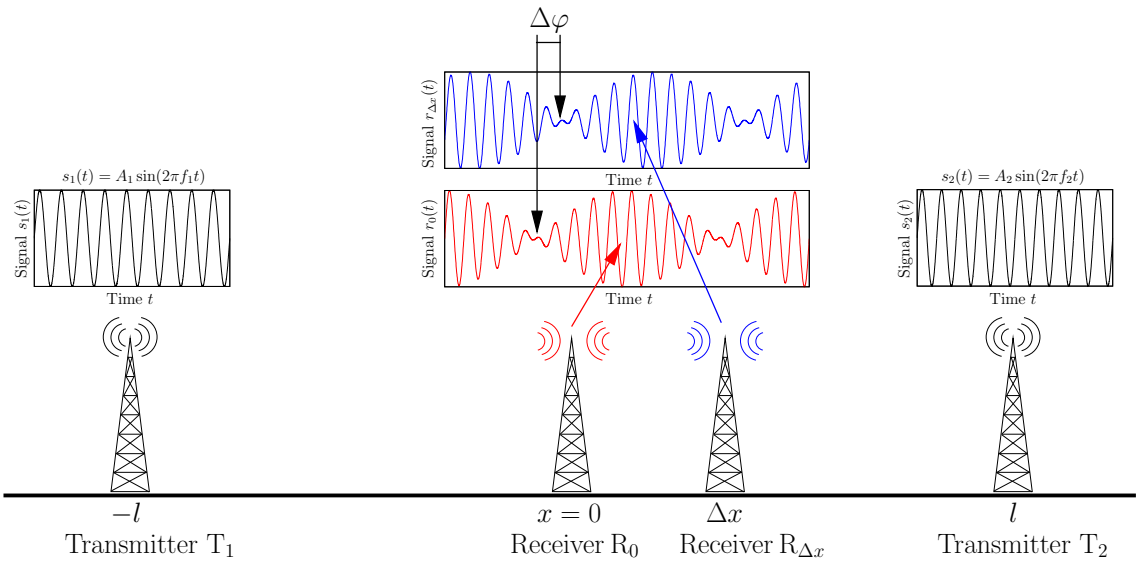

Figure 1. This analysis assumes a setup with two transmitter T_1 and T_2 as well as two receivers R_0 and $R_{\Delta x}$ that are located at $x = -l$, $x = l$, $x = 0$ and $x = \Delta x$, respectively. The figure also shows that both receivers sense a beat with a location-dependent phase-shift $\Delta\varphi$.

description of the actual procedure, as well as some of its properties.

2.1. Preliminaries

Most readers might know that if two transmitters emit sinusoidal signals, $s_1(t) = \sin(2\pi f_1 t)$ and $s_2(t) = \sin(2\pi f_2 t)$ with similar frequencies $f_1 \approx f_2$, these signals superpose, and a receiver will be reading the beat $r(t)$:

$$\begin{aligned} r_0(t) &= s_1(t) + s_2(t) \\ r_0(t) &= \sin\left(2\pi \frac{f_1 + f_2}{2} t\right) \cos\left(2\pi \frac{f_1 - f_2}{2} t\right) \end{aligned} \quad (1)$$

Figure 1 sketches a possible configuration for the appearance of beats. In this configuration, all the amplitudes and phase shifts are normalized such that Eq. (1) holds for the center position $x = 0$.

In addition, Figure 1 shows that at the off-center position $x = \Delta x$, a receiver $r_{\Delta x}(t)$ would observe a phase shift $\Delta\varphi$. Conversely, the phase-shift $\Delta\varphi$ can be used to derive the distance $\Delta x = \Delta\varphi c/(2\pi f_c)$ with $c \approx 3 \cdot 10^8$ m/s denoting the speed of light, and $f_c = (f_1 + f_2)/2$ denoting the carrier frequency. However, in order to make use of this phase shift, the receiver would require some global timing information. But nevertheless, it might be useful to realize that the phase shift can be derived at the *low-frequency* envelope signal.

2.2. The Procedure

The LSB procedure assumes the same physical setup as already described in Figure 1. But rather than emitting sinusoidal signals $s_i(t) = \sin(2\pi f_i t)$, the transmitters already emit beats of the form $b_i(t) = \sin(2\pi f_i t)\cos(2\pi f_m t)$ with slightly varying carrier frequencies f_i but identical envelopes '$\cos(2\pi f_m t)$'. At first glance, this little change seems tiny and negligible, but does have a major effect: the superposition of *properly configured beats* $b_1(t)$ and $b_2(t)$ leads to interferences with *location-dependent shapes*. Figure 2 illustrates this key feature: The middle part shows three different receivers at three different locations $\Delta x = 0$, Δx_1 and Δx_2. The envelopes at these three positions can be individually characterized by the three amplitudes A_1, A_2, and A_3. It can be clearly seen that the quotients A_1/A_2, A_1/A_3, A_2/A_3 vary from location to location. In other words, the receiver may detect the three amplitudes A_1, A_2, and A_3 in order to derive its location Δx from their quotients. More formally, a receiver $r_{\Delta x}(t)$ would read the following signal at location $x = \Delta x$:

$$\begin{aligned} r_{\Delta x}(t) &= \sin(2\pi f_1 t)\cos(2\pi f_m t) + \\ &\quad \sin(2\pi f_2 (t - \Delta t))\cos(2\pi f_m (t - \Delta t)) && (2) \\ \Delta t &= \frac{2\Delta x}{c} && (3) \\ f_1 &= f_g - \Delta f && (4) \\ f_2 &= f_g + \Delta f && (5) \\ f_m &= k|f_1 - f_2| \; ; \; k \in Q \; ; \; k \neq 1 && (6) \end{aligned}$$

In this description, Eq. (3) states that a location variation Δx affects the time-of-flight of the two beats $b_1(t)$ and $b_2(t)$ twice; a spatial shift increases the first one by $\Delta x/c$, and decreases the second one by the same amount. Eqs. (4) and (5) introduce the global carrier frequency f_g and the beat frequency Δf that both emerge from the superposition of the two carriers $f_1 \approx f_2$. Finally, Eq. (6) describes the relation between the emerging beat fre-

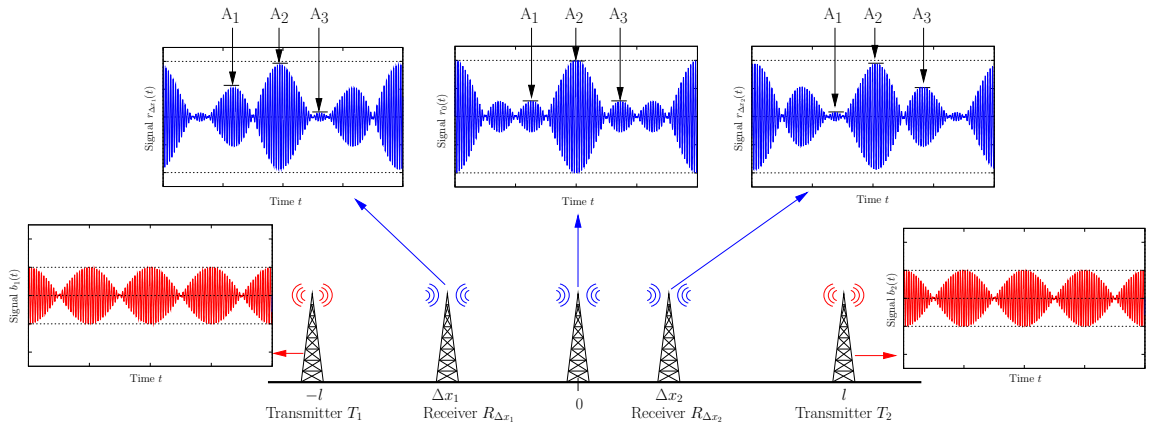

Figure 2. The superposing-beats procedure: two transmitter T_1 and T_2 emit modulated signals $b_{1/2}(t) = A_{1/2}\sin(2\pi f_{1/2}t)\cos(2\pi f_m t)$ as well as two receivers $R_{\Delta x_1}$ and $R_{\Delta x_2}$. The figure clearly shows that the two modulated carrier signals induces location-dependent interference patterns.

quency Δf and the modulation frequency f_m: in order to obtain stable, location-dependent interference patterns, the quotient of these two frequencies must be a rational number, preferably an integer, e.g., $f_m = n|f_1 - f_2|$ or $nf_m = |f_1 - f_2|$, respectively.

2.3. Some of the Procedure's Properties

Eq. (2) shows that at location $x = \Delta x$, a receiver reads the signal $r_{\Delta x}(t) = \sin(2\pi f_1 t)\cos(2\pi f_m t) + \sin(2\pi f_2(t-\Delta t))\cos(2\pi f_m(t-\Delta t))$. According to this equation, f_1, f_2, and f_m are system parameters that configure the procedure, and thus, its properties. In addition, these system parameters fulfill the constraints $f_m \ll f_1$ and $f_m \ll f_2$, which also holds for $\Delta f = (f_1 - f_2)/2$.

The last term of Eq. (2) can be rewritten as $\sin(2\pi f_2(t-\Delta t))\cos(2\pi f_m(t-\Delta t)) = \sin(2\pi f_2 t - \varphi_2)\cos(2\pi f_m t - \varphi_m)$ with $\varphi_2 = 2\pi f_2 \Delta t$ and $\varphi_m = 2\pi f_m \Delta t$ denoting the two phase shifts that appear due to the receiver's off-center position. A comparison of $\varphi_2 \gg \varphi_m$ suggests that φ_2 reacts very sensitively to a location shift Δx, whereas φ_m remains almost constant, and thus still provides a constant reference signal. The differences in the location sensitivity provide a good indication for why the envelope's shape, i.e., A_1, A_2, and A_3, changes when going from one location to another. These changes were already shown in Figure 2 and are highlighted in Figure 3 as well as directly compared in Figure 4. These figures also clearly show that the determination of the relations $A_i/A_{i\neq j}$ can be done on the low-frequency envelope as opposed to the high-frequency carrier signal $f_g(t)$.

The global carrier frequency $f_g = (f_1 + f_2)/2$, which is close to the two carriers $f_1 \approx f_g$ and $f_2 \approx f_g$, determines the procedure's resolution. At location $x = \Delta x$, for example, the phase shift is $\varphi_g = 2\pi f_g \Delta t$. By inserting Eq. (3) and then solving for Δx, this equation can be rewritten as:

$$\varphi_g = \frac{4\pi f_g \Delta x}{c} \,. \tag{7}$$

This equation shows that both the carrier frequency f_g and the resulting phase shift φ_g are linearly coupled. Assume, for example, that by means of the amplitudes $A_1 \ldots A_3$ and potentially other data, the receiver can detect a phase shift of $\Delta\varphi = 1°$. Then, a carrier of approximately 84 MHz would suffice to obtain a precision of 1 cm.

The procedure uses only periodic signals (see also Eq. (2)). Therefore, its behavior, and the envelope in particular, can be expected to be periodic as well. In a first approximation, the envelope's period time T_s (see, also, Figure 3) is defined by Δf, since a time shift Δt is much more significant with respect to f_1 and f_2 as compared to f_m.

Due to the lack of a theoretical analysis, this paper uses some numerical simulations to investigate the periodic behavior of the LSB procedure. The results are summarized in Table 1. This means that measurements of Δx are bound by the period T_s. For extended effective ranges, the procedure has to count the number of periods as is also done, for example, in a laser interferometer.

2.4. The Procedure's Periodic Behavior

The LSB procedure is based on periodic signals. It is thus interesting to determine the procedure's overall range for Δx after which it repeats the pattern of its signal $r_{\Delta x}(t)$. To this end, this subsection considers the cases of Δt at which the resulting phase shifts assume the dedicated values $\varphi_{m/2} = [0, \pi/2, \pi, 3/2\pi, 2\pi]$. With respect to f_m, the following cases can occur:

$$\underline{\varphi_m = 2\pi f_m \Delta t = 0}$$
$$r(t) = \cos(2\pi f_m t)(\sin(2\pi f_1 t) + \sin(2\pi f_2 t)) \tag{8}$$
$$\underline{\varphi_m = 2\pi f_m \Delta t = \pi/2}$$
$$r(t) = \sin(2\pi f_1 t)\cos(2\pi f_m t) +$$

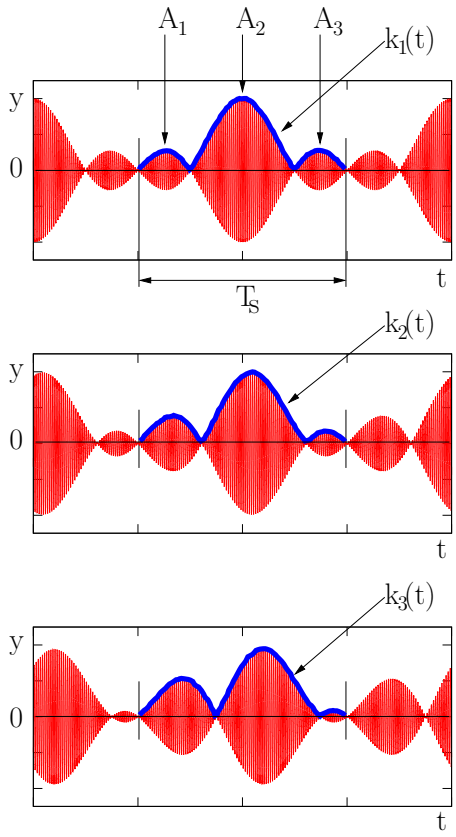

Figure 3. The envelope's actual shape depends on the location Δx.

$$\sin\left(2\pi f_2 t - \frac{1}{2}\pi\frac{f_2}{f_m}\right)\sin(2\pi f_m t) \quad (9)$$

$\underline{\varphi_m = 2\pi f_m \Delta t = \pi}$

$$r(t) = \cos(2\pi f_m t)\,(\sin(2\pi f_1 t) - \sin\left(2\pi f_2 t - \pi\frac{f_2}{f_m}\right)\Big) \quad (10)$$

$\underline{\varphi_m = 2\pi f_m \Delta t = 3/2\pi}$

$$r(t) = \sin(2\pi f_1 t)\cos(2\pi f_m t) -$$

Table 1. Numerical experiments indicate that the envelope's period time T_s depends on f_g, Δf and f_m.

f_g in Hz	Δf in Hz	f_m in Hz	T_s in s
100	1	0.4	5.0
100	1	0.5	2.0
100	1	0.6	2.5
100	2	0.4	1.25
100	2	0.5	2.0
100	2	0,6	5.0
500	1	0.5	2.0
650	1	0.5	2.0
1000	1	0.5	2.0

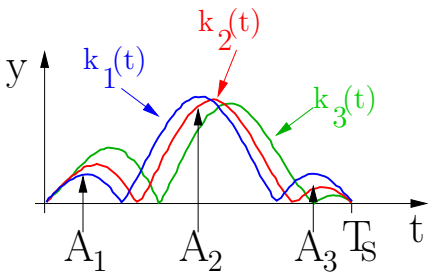

Figure 4. This figure shows the three envelopes $k_1(t)$, $k_2(t)$, and $k_3(t)$ as already presented in Figure 3.

$$\sin\left(2\pi f_2 t - \frac{3}{2}\pi\frac{f_2}{f_m}\right)\sin(2\pi f_m t) \quad (11)$$

$\underline{\varphi_m = 2\pi f_m \Delta t = 2\pi}$

$$r(t) = \cos(2\pi f_m t)\,(\sin(2\pi f_1 t) + \sin\left(2\pi f_2 t - 2\pi\frac{f_2}{f_m}\right)\Big) \quad (12)$$

These equations indicate that the pattern is repetitive if f_2/f_m is odd. In this case equation 8 is equal to 10. With respect to f_2, the repetition occurs at $\Delta t = n/f_2$ for $2\pi f_2 \Delta t$ by $n \in N$ as Eqs. (13) to (17) show. These equations assume the realistic relation $f_m \ll f_2$ for which the ratio $f_m/f_2 \approx 0$ vanishes.

$\underline{\varphi_2 = 2\pi f_2 \Delta t = 0}$

$$r(t) = \cos(2\pi f_m t)(\sin(2\pi f_1 t) + \sin(2\pi f_2 t)) \quad (13)$$

$\underline{\varphi_2 = 2\pi f_m \Delta t = \pi/2}$

$$r(t) = \sin(2\pi f_1 t)\cos(2\pi f_m t) - \cos(2\pi f_2 t)\cos\left(2\pi f_m t - \frac{1}{2}\pi\frac{f_m}{f_2}\right) \quad (14)$$

$\underline{\varphi_2 = 2\pi f_m \Delta t = \pi}$

$$r(t) = \sin(2\pi f_1 t)\cos(2\pi f_m t) - \sin(2\pi f_2 t)\cos\left(2\pi f_m t - \pi\frac{f_m}{f_2}\right) \quad (15)$$

$\underline{\varphi_2 = 2\pi f_m \Delta t = 3/2\pi}$

$$r(t) = \sin(2\pi f_1 t)\cos(2\pi f_m t) + \cos(2\pi f_2 t)\cos\left(2\pi f_m t - \frac{3}{2}\pi\frac{f_m}{f_2}\right) \quad (16)$$

$\underline{\varphi_2 = 2\pi f_m \Delta t = 2\pi}$

$$r(t) = \sin(2\pi f_1 t)\cos(2\pi f_m t) + \sin(2\pi f_2 t)\cos\left(2\pi f_m t - \pi\frac{f_m}{f_2}\right) \quad (17)$$

A specific system can be expected to differentiate patterns in the range $0 \leq \varphi < 2\pi f_2 \Delta t = 2\pi$. For example, a frequency of 100 MHz for f_2 results in an effective range of $\Delta s \approx 3\,m$.

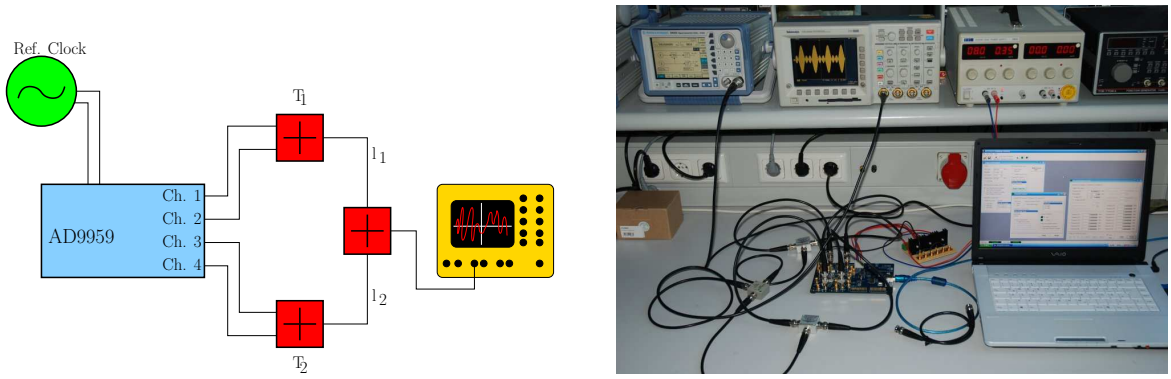

Figure 5. The left-hand-side shows the schematically the setup of the experiment in which a DDS-Chip AD9959 generates four reference signals. Two mini-circuit combiners ZFSC-2-1 generate the actual beats $b_1(t)$ and $b_2(t)$. A third combiner simulates a receiver and displays its signal readings $r_{\Delta x}(t)$ on a Tektronix TDS 3034 oscilloscope. The right-hand-side shows the actual laboratory equipment.

3. Experimental Validation

Figure 5 shows both the structural and the actual laboratory setup that was used for the validation of the theoretical concepts of the LSB procedure. The setup consists of a 4-channel direct digital synthesizer (DDS) and a receiver. In order to focus on the *functional* aspects, the receiver was simulated by means of cables and a combiner, which displays its signal readings on a Tektronix TDS 3034 oscilloscope.

Since, the AD9959 synthesizer is not able to generate the two beats $b_1(t)$ and $b_2(t)$ directly, they had to be generated indirectly as follows: On its four channels, the chip generates sinusoidal signals with the frequencies:

Ch_1	=	F + 3.77 Hz	Ch_2	=	F + 0.05 Hz
Ch_3	=	F - 7.40 Hz	Ch_4	=	F - 3.68 Hz

with F=50 MHz denoting a global, high-frequency carrier. Like the generation of simple beats (see also Subsection 2.1), two mini-circuit combiners ZFSC-2-1, T_1 and T_2, generated the two beats by superposing pairs of these channels. The two carrier frequencies are $f_1 = 0.5(\mathrm{Ch}_1 + \mathrm{Ch}_2) = F + 1.91\,\mathrm{Hz}$ and $f_2 = 0.5(\mathrm{Ch}_3 + \mathrm{Ch}_4) = F - 5.54\,\mathrm{Hz}$. In both cases, the modulation frequency is $f_m = 0.5(\mathrm{Ch}_1 - \mathrm{Ch}_2) = 0.5(\mathrm{Ch}_3 - \mathrm{Ch}_4) = 1.86\,\mathrm{Hz}$. With $\Delta f = 0.5(f_1 - f_2) = 3.725\,\mathrm{Hz}$, the konstant k (see Eq. (6)) equals to $k = f_m/\Delta f = 0.5$. In summary:

f_1	=	F + 1.91 Hz	f_2	=	F - 5.54 Hz
f_m	=	1.86 Hz	f_g	=	F - 1.815 Hz
Δf	=	3.725 Hz	k	$\approx$	0.5

Figure 6 shows the signals $r_{\Delta x}(t)$ with $\Delta x = |l_1 - l_2|$ whereas l_2 was changed by various cable lengths. The receiver would read at the four distance differences $\Delta x \approx 0\,\mathrm{cm}$, $\Delta x \approx 50\,\mathrm{cm}$, $\Delta x \approx 100\,\mathrm{cm}$, and $\Delta x \approx 150\,\mathrm{cm}$, respectively. It can be clearly seen that each of the plots displays interference patterns with significantly different shapes. Furthermore, the plots validate the simulation data already shown in Figures 2-4.

4. The Detector

For obvious reasons, the procedure requires a detector. Its goal is to derive the location Δx by analyzing the incoming signal. Figure 7 sketches a rather generic implementation that consists of the following four components:

1. A high-frequency receiver that is tuned to f_g.
2. A peak detector that extracts the signal's envelope.
3. A digitizer that does the analog-to-digital conversion required by further processing stages.
4. A software processor that by knowing f_g, Δf, and f_m, estimates the time shift Δt, and thus, the relative location Δx.

For the derivation of the time shift Δt, the detector has different options. First of all, it can try to directly solve the inherent sin/cos-equations. A second option consists in applying a cross-correlation with pre-processed envelopes that refer to different locations Δx. But with respect to the actual implementation, the main advantage is that the sampling can be done on the low-frequency envelope.

5. Conclusions

This paper has presented a novel method for measuring the relative distance with respect to at least two transmitters. These transmitters emit beats with slightly varying carrier frequencies but equivalent envelopes. At

$\Delta x \approx 0$ cm:

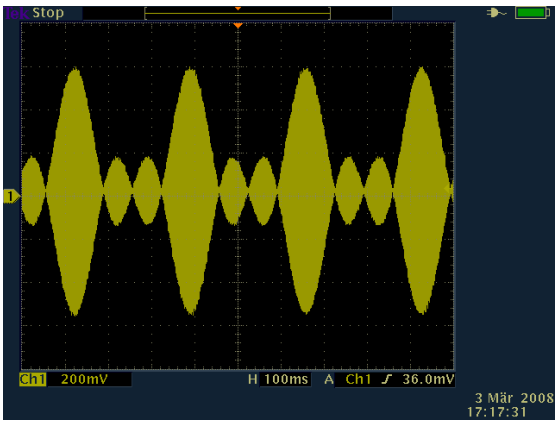

$\Delta x \approx 50$ cm:

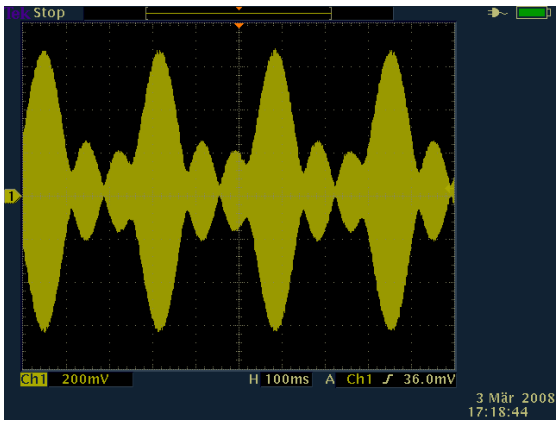

$\Delta x \approx 100$ cm:

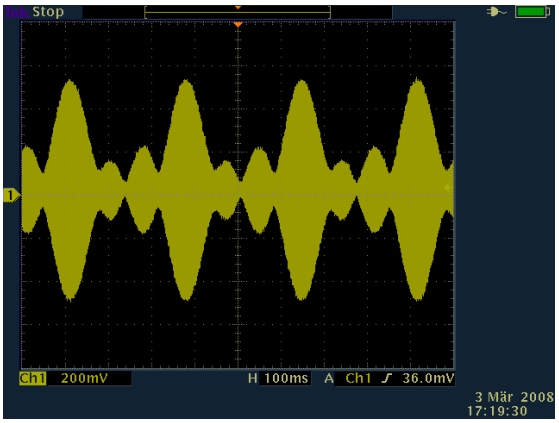

$\Delta x \approx 150$ cm:

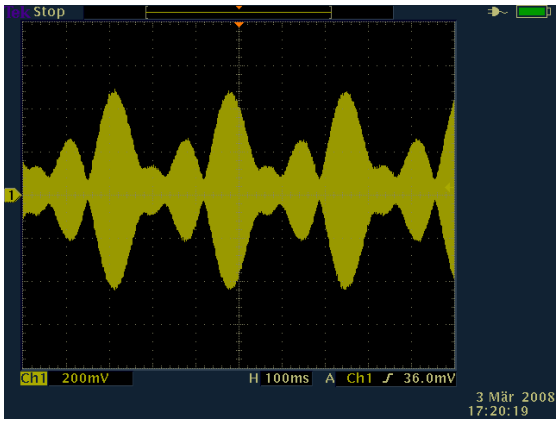

Figure 6. This figure shows the signals $r_{\Delta x}(t)$ a receiver would read at the four distance differences $\Delta x \approx 0$ cm, $\Delta x \approx 50$ cm, $\Delta x \approx 100$ cm, and $\Delta x \approx 150$ cm.

the receiver's side, these beats superpose from which a location-dependent interference pattern emerges. The low-frequency envelope patterns are then subject to further processing stages that derive the receiver's relative location Δx.

The proposed localization method has two key advantages. First, the transmitters' carrier frequencies determine the obtainable resolution. Second, the receiver has to analyze only the low-frequency envelope, which is in way contrast to other methods, which normally require access to the high-frequency components.

In addition, this paper has presented the results of some validation experiments. The next step of the experiment assembly is to switch to a wireless setup in which a peak-detector (or envelope tracker) analyzes the actual envelope.

Future research will also be devoted to a thorough theoretical analysis. This analysis aims to clearer understand the procedure as well as to find a simple means for the derivation of the location Δx.

In addition, future research will also employ the time-of-arrival of certain signals in order to significantly increase the procedure's effective range of operation. Since this additional component will be responsible only for some wide range estimates, the required electrical parts can be rather simple, and thus, cheap.

6. Acknowledgements

The authors gratefully thank Dr. D. Birus of the Max-Planck-Institut for Plasmaphysics in Greifswald for his valuable discussions about signal theory and his active help in designing the experimental setup.

References

[1] http://www.indoorgps.com.

[2] I. F. Akyildiz, Y. S. W.Šu, and E. Cayirci. A survey on sensor networks. *IEEE Communication Magazine*, pages 102–114, 2002.

[3] J. Blumenthal, F. Reichenbach, and D. Timmermann. Minimal transmission power vs. signal strength as distance estimation for localization in wireless sensor networks. *International Workshop on Wireless Ad-hoc and Sensor Networks (IWWAN'06)*, June 2006.

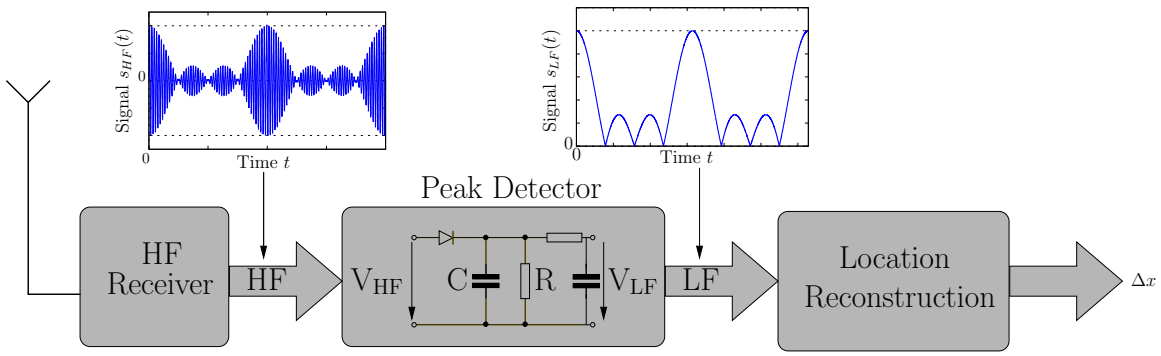

Figure 7. This figure shows a block diagram for the detector.

[4] E. D. Kaplan. *Understanding GPS: Principles and Applications*. Artech House Publishers, 1996.

[5] M. O. Kechine, C. C. J. M. Tiberius, and H. van der Marel. Network differential gps: Kinematic positioning with nasa's internet-based global differential gps. *Journal of Global Positioning Systems*, 2(2):139–143, 2003.

[6] M. Maroti, B. Kusy, G. Balogh, P. Volgyesi, A. Nadas, K. Molnar, S. Dora, and A. Ledeczi. Radio interferometric geolocation. *In Proceedings of the 3rd ACM Conference on Embedded Networked Sensor Systems*, November 2005.

[7] D. Moore, J. Leonard, D. Rus, and S. Teller. Robust distributed network localization with noisy range measurements. *In Proceedings of the Second ACM Conference on Embedded Networked Sensor Systems*, pages 50–61, November 2004.

[8] R. Salomon. Precise position learning in coarse-grained localization algorithms. *Proceedings of the IEEE SECON'05 Conference*, 2005.

[9] F. van Diggelen and C. Abraham. *Indoor GPS Technology*. Presented at CTIA Wireless-Agenda, Dallas, May 2001.